

Superconducting Kinetic-Inductance Microwave Filters

Kenneth R. Carroll, Jeffrey M. Pond, and Edward J. Cukauskas

Abstract—Several kinetic-inductance microstrip filters have been designed and tested. The microstrip consists of a superconducting niobium carbon nitride (NbCN) strip separated from a NbCN ground plane by an amorphous hydrogenated-silicon dielectric. The circuits investigated include an interferometer, a stepped-impedance, a low-frequency stub, and a high-frequency stub filter. Generally, for frequencies below 20 GHz, good transmission characteristics were measured for these structures. A simple physical model is used to determine the major features of the transmission characteristics over a wide temperature and frequency range. Other important issues such as the superconductor and dielectric losses, impedance matching, and film uniformity are addressed for these structures.

I. INTRODUCTION

FOR microwave systems, filters are an important class of circuits. Besides their obvious application of providing frequency selectivity, they are necessary for matching networks which form an integral part of multiplexers, negative resistance, and parametric amplifiers, to mention a few. The use of superconducting transmission lines in the design of these microwave devices provide several benefits over their normal-metal counterparts. The primary advantages are a frequency independent penetration depth and low surface resistance which allow the implementation of compact designs with low insertion loss, large bandwidth, and low dispersion. Additional reductions in device size can be realized by using superconducting microstrip operating in the kinetic-inductance limit [1], [2], [4]. This limit occurs when the thicknesses of the superconducting and dielectric films are less than the penetration depth [5], [6]. For passive microwave circuits where the lengths of the resonant elements are integral multiples of a half-wavelength, the size reduction can be substantial while an acceptable level of loss is maintained.

In this paper, four filters using superconducting microstrip line are reported on. The measured microwave response of the devices are compared to the predicted response using the physical model described below. In Fig. 1(a)–(d), the circuits tested are shown which include an interferometer, a stepped-impedance, a low-frequency stub, and a high-frequency stub filter, respectively. A

coplanar transition region provides the electrical connection between 50- Ω coax cables and the microstrip lines. The filter geometry is defined by the patterned top superconductor layer. The deposition and processing steps for the niobium carbon nitride (NbCN), amorphous hydrogenated silicon (a-Si::H), and NbCN trilayers will be given in the next section. Although trilayer transmission lines have been fabricated in high-temperature superconductors [7], presently, the microwave losses are higher than for the more traditional materials where low-loss circuits have been successfully fabricated [1], [2], [4].

The microstrip lines in Fig. 1 are $\sim 10 \mu\text{m}$ wide and the dielectric film thicknesses are $\sim 0.1\text{--}0.3 \mu\text{m}$ giving an aspect ratio of $\sim 30\text{--}100$. Consequently, a parallel plate transmission-line analysis is valid. The coupling between adjacent lines, which is proportional to the dielectric thickness over the separation, is negligible. The small dielectric thickness allows the microstrip lines to be placed in close proximity to one another yielding ultra-compact designs. One should also note that even though the superconducting films are substantially thinner than a penetration depth, the electromagnetic energy outside of the line is orders of magnitude less than that of the guided signal. The vast difference between the thickness of the deposited dielectric and the substrate thickness results in this distribution of the energy [8].

This investigation was undertaken to address several issues regarding the practicality of using kinetic-inductance microstrip in complex circuit topologies. One of the major concerns is the matching of the extremely small cross-sectional geometries of the kinetic-inductance microstrip to standard 50- Ω components. Another concern is the spatial thickness variations inherent in any deposition process, since the propagation constant of the microstrip is very dependent on the thicknesses of the films (see (3)). These variations will impose limitations on the types of designs that can be realized. To more easily determine the design limitations, the circuits used two sets of identical elements rather than implementing a Chebyscheff, elliptical, or other traditional responses which require additional elements. By restricting the number of elements, the photolithography is simplified since the correct impedance ratios between the elements is less critical.

To quantitatively model the transmission characteristics of these designs, the superconducting and dielectric films need to be characterized. The parameters needed for the

Manuscript received January 3, 1992; revised October 15, 1992. This work was supported by the Office of Naval Technology. One of the authors (KRC) held a Naval Research Laboratory/National Research Council research associateship during the course of this work.

The authors are with the Electronics Science and Technology Division, Naval Research Laboratory, Washington, DC 20375
IEEE Log Number 9206225.

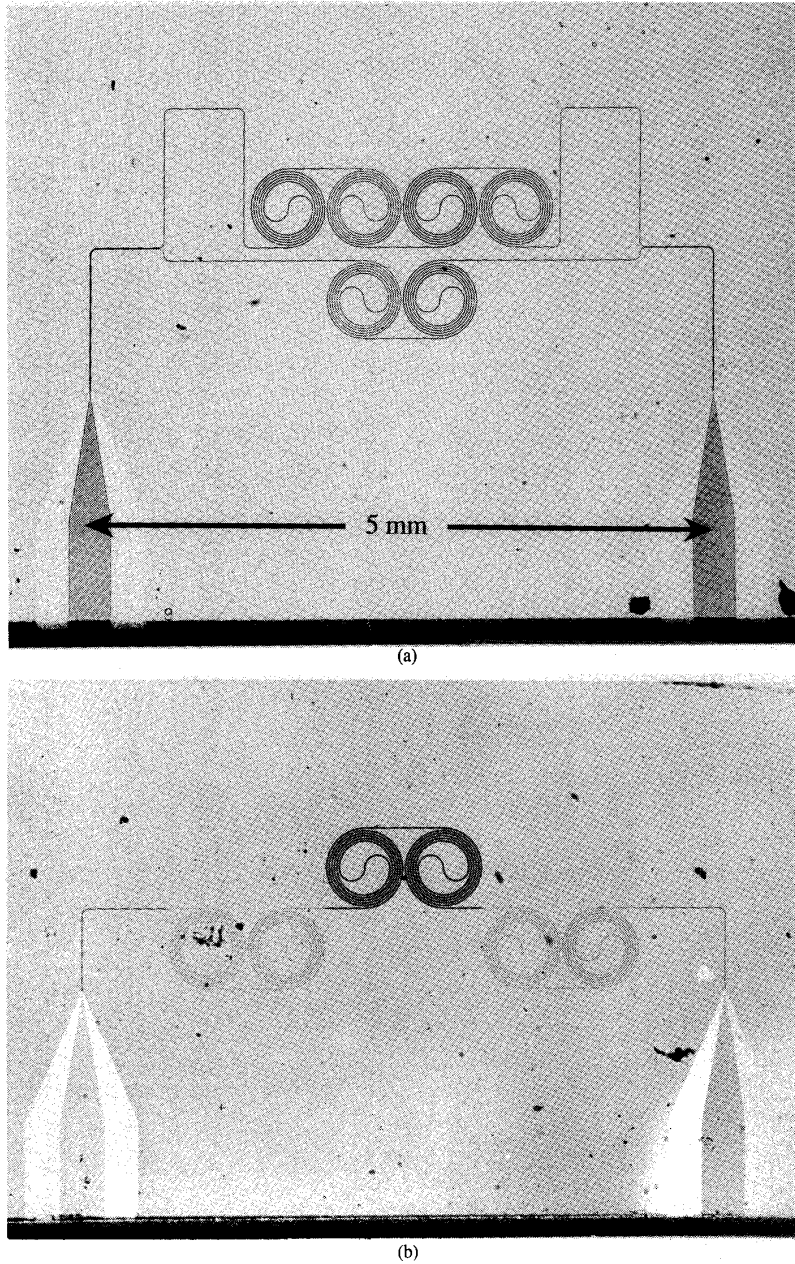


Fig. 1. Photographs of the interferometer (a), stepped-impedance filter (b), low-frequency stub filter (c), and high-frequency stub filter (d) (c and d on facing page).

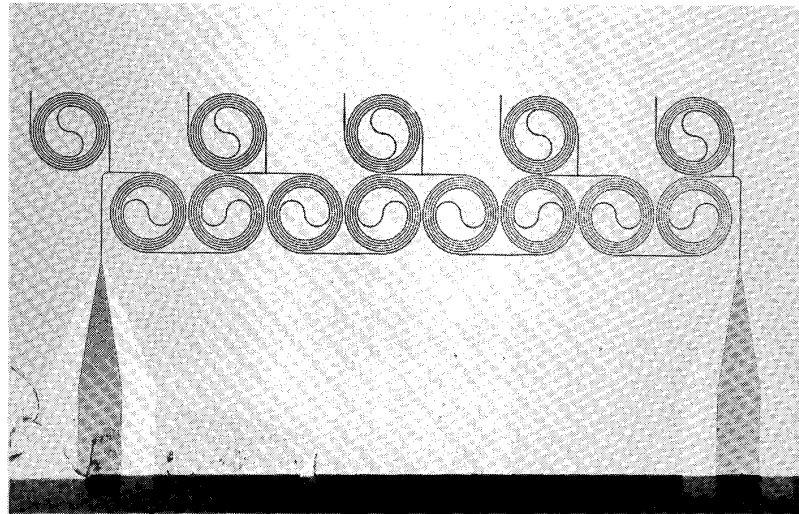
superconducting films are the thickness d_s , critical temperature T_c , zero-temperature penetration depth λ_0 , and the normal-state conductivity σ_n . For the dielectric film, one needs the thickness d_d , the relative dielectric constant ϵ_r , and the loss tangent $\tan \delta$. For NbCN, the penetration depth is reasonably well characterized by the Gorter-Casimir equation [5]

$$\lambda = \frac{\lambda_0}{\sqrt{1 - (T/T_c)^4}} \quad (1)$$

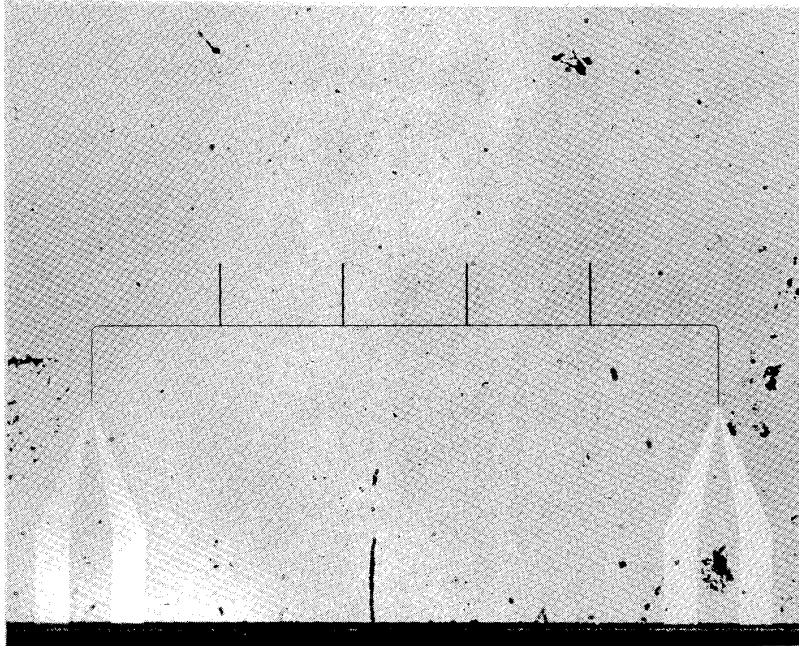
where T is the temperature of the film. The effective conductivity σ due to the quasiparticle density of electrons in the superconductor has a temperature dependence given by [5]

$$\sigma = \sigma_n \left(\frac{T}{T_c} \right)^4 \quad (2)$$

When the thicknesses of the dielectric and superconducting films are on the same order or less than the



(c)



(d)

Fig. 1. (Continued).

penetration depth, the effective inductance resulting from the energy stored in the kinetic motion of the Cooper pairs and the energy stored in the superconducting films is comparable to or greater than the inductance resulting from the energy in the dielectric. Since the phase velocity is given by $v_p = 1/(LC)^{1/2}$ where L is the inductance per unit length and C is the capacitance per unit length, this additional inductance results in a slowing of the applied signal. In the parallel-plate approximation, the explicit dependence of the phase velocity on the penetra-

tion depth and the film thicknesses is [5], [6]

$$v_p = \frac{c}{\sqrt{\epsilon_r}} \frac{1}{\sqrt{1 + 2(\lambda/d_d) \coth(d_s/\lambda)}} \quad (3)$$

where c is speed of light in vacuum and the superconductors are assumed to be identical. The first term underneath the radical is due to the magnetic energy stored in the dielectric while the second term results from the additional inductance usually referred to as the kinetic inductance [5]. A factor of 30 slowing due to the kinetic

inductance has been demonstrated [1], [2]. Since distributed microstrip circuits are planar, the size reduction due to kinetic inductance effects can vary from $(\epsilon_r)^{1/2}v_p/c$ for a delay line to $\epsilon_r(v_p/c)^2$ for a complex two-dimensional topology. An additional factor of 1.5–5 in slowing results from the value of the relative dielectric constant.

In addition to the phase velocity, an equally important issue for any microwave device is its insertion loss when it is integrated into a circuit. Insertion loss can result from impedance mismatch, geometric discontinuities, and attenuation loss. In the parallel-plate limit, the characteristic impedance of a superconducting microstrip is given by [6]

$$Z_c = \frac{d_d}{w} \sqrt{\frac{\mu_0 [1 + 2(\lambda/d_d) \coth(d_s/\lambda)]}{\epsilon_0 \epsilon_r}} \quad (4)$$

where w is the width of the line, μ_0 is the permeability of free space, and ϵ_0 is the permittivity of free space. By proper design, this impedance can be matched to a standard 50- Ω system either by the proper choice of the parameters in (4) or by the use of an impedance transformer.

The geometric discontinuity involved in the transition from the kinetic-inductance microstrip to 50- Ω coax presents a challenging design problem. The approach pursued in this investigation is to employ a ‘‘coplanar’’ waveguide section, shown in Fig 1(a)–(d), between the coax and kinetic-inductance microstrip. The center conductor of the coplanar waveguide linearly tapers down from where contact with the coax center conductor is made to the width of the microstrip. The two common outer conductors of the coplanar region are connected to the outer conductor of the coax at the edge of the substrate and then taper linearly and merge to become the ground plane of the microstrip at a point where the center conductor crosses over, separated by the thin-film dielectric. Although geometrically similar to the impedance transformer investigated by McGinnis *et al.* [9], the tapered coplanar region is used here to connect two transmission lines with similar impedances but drastically different field patterns.

Insertion loss due to dissipation in the microstrip lines can result from either losses in the dielectric or quasiparticle conduction in the superconducting films. The loss constant for the dielectric is

$$\alpha_d = \frac{\pi f}{v_p} \tan \delta \quad (5)$$

where f is the frequency while the loss constant of the superconducting films is given by [6]

$$\alpha_s = \frac{(2\pi f)^2 \lambda^3 \mu_0 \epsilon_r \sigma v_p}{2d_d c^2} \cdot \left[\coth(d_s/\lambda) + \frac{d_s}{\lambda} \sinh^{-2}(d_s/\lambda) \right]. \quad (6)$$

A more convenient figure of merit for transmission line loss is the quality factor which is the ratio of the energy stored in the electromagnetic signal to the amount of energy lost per cycle. This quantity is given by $Q_{s,d} = \pi f / v_p \alpha_{s,d}$. For the superconducting microstrip line, a total quality factor can be defined as $Q \equiv (1/Q_d + 1/Q_s)^{-1}$. In the thin-film limit ($d_s, d_d \ll \lambda$), the superconductor quality factor simplifies to

$$Q_s = \frac{1}{2\pi f \mu_0 \sigma \lambda^2} \quad (7)$$

which is essentially the square of the ratio of the classical skin depth to the penetration depth. Since this expression is independent of the film thicknesses, additional slowing can be achieved by using thinner films without incurring additional loss. In the thick-film limit ($d_s, d_d \gg \lambda$), the quality factor is increased by the ratio d_d/λ over that given by (7).

In Fig. 2, the superconducting quality factor is shown as a function of frequency for the reduced temperatures T/T_c of 0.3, 0.5, 0.8, and 0.95 in the thin-film limit. The values used for the penetration depth and normal-state conductivity are $\lambda_0 = 0.4 \mu\text{m}$ and $\sigma_n = 10^6 (\Omega\text{m})^{-1}$, respectively which are reasonable values for NbCN films [1], [2], [4]. For these values, one obtains quality factors greater than 100 below 10 GHz and a reduced temperature of 0.8. While for some applications a quality factor of 100 may be acceptable, dielectric quality factors as high as 10^5 could be expected since these have been obtained for bulk materials [10]. For $Q_d = 10^5$, one is limited by the superconductor losses for most of the frequency and temperature range shown in Fig. 2. However, a relatively high overall Q of 10^3 is maintained up to 10 GHz for a reduced temperature of $0.5 T_c$.

II. FABRICATION PROCESS AND EXPERIMENTAL DETAILS

The trilayer structures were fabricated in an ultra high-vacuum sputtering system [11]. The films were grown on quartz substrates with dimensions of $2.5 \times 2.5 \times 0.1\text{-cm}^3$. The ground plane was first deposited by rf sputtering a 15 cm-diameter Nb target in an argon (84%), nitrogen (13%), and methane (3%) gas mixture with a substrate temperature of approximately 600 °C and the rf power density of 4.3 W/cm². Without breaking vacuum, half the hydrogenated-silicon dielectric layer was then deposited by sputtering a silicon target in an argon (85%) and hydrogen (15%) gas mixture with an rf power density of 0.85 W/cm². The sample was then removed from the system to pattern the ground-plane layer. After etching the films in a barrel plasma etcher, the remaining half of the hydrogenated silicon was deposited followed by the top NbCN film. The deposition of the silicon layer in two steps was done to minimize the possibility of pin-hole shorts between the two superconducting layers. The top film was patterned using a parallel-plate reactive ion etcher to define the microstrip lines. The thickness of the

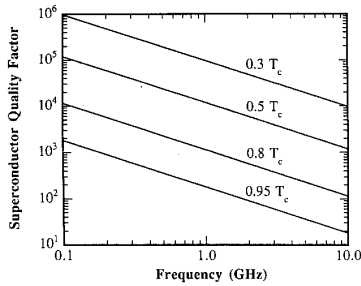


Fig. 2. Superconductor quality factor versus frequency for a microstrip line at the reduced temperatures of 0.3, 0.5, 0.8, and 0.95. The curves are in the thin-film limit with $\lambda_0 = 0.4 \mu\text{m}$ and $\sigma_n = 10^6 (\Omega\text{m})^{-1}$.

NbCN films (which in our previous work were referred to as niobium nitride films [1], [2], [4]) were 25 nm and the a-H::Si films were either 100 nm or 300 nm.

To determine the microwave properties of the circuits, the substrate was mounted on a test fixture which used 0.034-inch diameter coaxial cable. The coplanar transition regions were connected to the coax in one of two methods. For one method, silver epoxy was spread over a portion of the transition-region center conductor and ground plane. Pressure contact was then made to the contact points. For the other method, part of the transition region center conductor and ground plane were coated with 10 nm of Cr followed by 300 nm of gold using a photoresist liftoff technique. A 25- μm diameter gold wire was then bonded to the areas and silver epoxy was typically applied at the bonding points to improve mechanical stability.

With the sample mounted, the test fixture was placed in the experimental space of a liquid helium cryostat. The rf electrical connection between the room-temperature electronics and the test fixture was made by 0.085-inch 50- Ω stainless-steel coax cables with a 1.25-m length. The magnitude of the transmission coefficient $|S_{21}|$ of the filters was measured with a Hewlett Packard 8510 vector network analyzer. The attenuation of the applied signal due to the coax cables of the probe and room-temperature electronics were calibrated out of the measurements.

III. CIRCUIT MODELING

One of the goals of this investigation is to demonstrate that these structures can be fabricated with sufficient accuracy that they can be modeled by incorporating superconducting parallel-plate transmission-line equations into standard microwave CAD tools. To prove that this goal can be accomplished, the inverse problem is addressed. That is, from the measured transmission characteristics, the materials properties of the superconducting and dielectric films are determined for several devices and shown to be consistent. The degree of consistency will of course be limited by the physical model assumed, the sensitivity of the device characteristics to the material properties, and processing defects in the microstrip lines.

Modeling of these circuits was facilitated by Eesof's

microwave-circuit analysis package. The superconducting transmission lines were modeled using a general transmission-line element that could incorporate (1)–(6) in a straightforward manner. The circuit models included a series parasitic inductance and capacitance at the input and output of the filters. These parasitics were included to account for the rf connections between the 50- Ω coax cables and the superconducting films of the filters. The parasitic inductance also accounts for the effects of the coplanar transition region as discussed in Section IV-B.

The circuit analysis program allows the determination of the penetration depth, critical temperature, and loss parameters by comparison of the computed and measured transmission characteristics. Simple visual comparison of the experimental and theoretical graphs results in reasonably accurate values for the film parameters. Further numerical optimization can be done to improve the results. The optimization function used for the numerical analysis was the sum of the transmission coefficients in dB over all frequencies. The difference between the measured and computed functions is then minimized using a gradient search of the parameter space. This logarithmic form for the minimization function equally weights the passbands and nulls.

An efficient way to determine the materials parameters is to first determine the penetration depth and the loss tangent at a temperature well below the critical temperature where both the critical temperature and normal-state conductivity have a negligible effect on the transmission characteristics as indicated by (1) and Fig. 2. Then the critical temperature and normal-state conductivity are found by fitting data near the critical temperature. As a consequence of this approach, the model is least accurate at intermediate temperatures where the measured phase velocity is slightly lower than the predicted value using the Gorter–Casimir dependence.

The other parameters such as the parasitic capacitances and inductances can be optimized at any temperature. Once the final parameters are determined, one only needs to change the temperature to produce the curve fit for the measured transmission data.

IV. RESULTS

A. Material Properties

In Figs. 3–6, the magnitude of the transmission characteristics $|S_{21}|$ of the interferometer, stepped-impedance, low-frequency stub, and high-frequency stub filter, are shown, respectively. For each temperature, the solid line indicates the measured data and the dashed line the optimized results of the models. A reasonable agreement between the model and measurements over as broad a frequency range as possible was sought rather than the demonstration of an excellent fit over a narrow frequency range. For the devices, the NbCN and dielectric film thicknesses were 25 nm and 300 nm, respectively. In Table I, the lengths and nominal widths of the resonant elements are given. Generally, the microstrip lines were

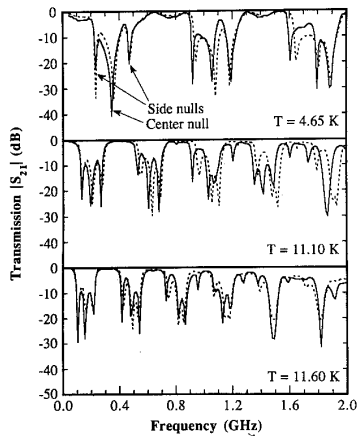


Fig. 3. Interferometer transmission data (solid lines) for the temperatures of 4.65 K, 11.1 K, and 11.6 K. The dashed lines represent the fitted curves. The model was fitted over as large a frequency and temperature range as possible for which a reasonable fit could be achieved rather than optimizing the fit over a single passband.

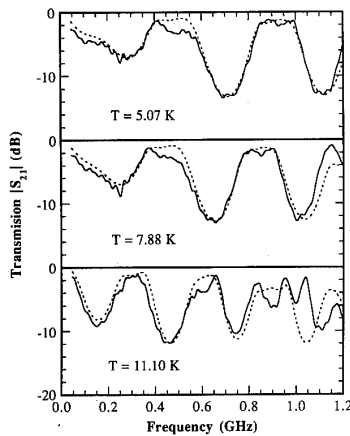


Fig. 4. Stepped-impedance filter transmission data (solid lines) for the temperatures 5.07, 7.88, and 11.1 K. The dashed lines represent the fitted curves. The model was fitted over as large a frequency and temperature range as possible for which a reasonable fit could be achieved rather than optimizing the fit over a single passband.

slightly thinner than these values due to the lithographic processing. For ϵ_r , a value of 10.5 was assumed [2]. The measured line widths were used in the models.

As can be seen from the graphs, the model after optimizing the circuit parameters predicts the transmission characteristics very well. Especially good agreement is obtained for the interferometer where each stopband has a center and two side nulls. The center null results when the difference in lengths between the short and long arm are half a wavelength, and the side nulls are due to reflections from an impedance mismatch between the arms and the trunkline. For the four devices, the resulting penetration depth, critical temperature, loss tangent, inverse of the superconductor quality factor, and normal-state conductivity are summarized in Table II. The super-

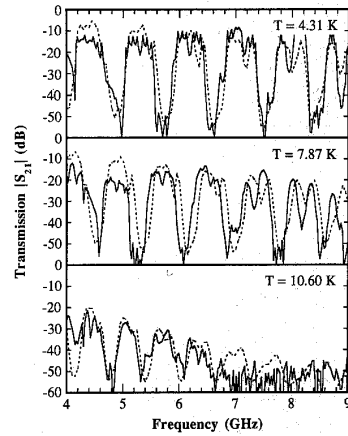


Fig. 5. Low-frequency stub filter transmission data (solid lines) for the temperature 4.31, 7.87, and 10.60 K. The dashed lines represent the fitted curves. The model was fitted over as large a frequency and temperature range as possible for which a reasonable fit could be achieved rather than optimizing the fit over a single passband.

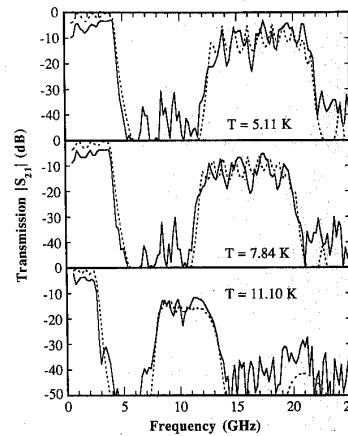


Fig. 6. High-frequency stub filter transmission data (solid lines) for the temperatures 5.11, 7.84, and 11.10 K. The dashed lines represent the fitted curves. The model was fitted over as large a frequency and temperature range as possible for which a reasonable fit could be achieved rather than optimizing the fit over a single passband.

conductor quality factor was computed for a frequency of 1 GHz and a temperature of 4.2 K. Also for comparison purposes, the previous results reported for a high-frequency stub filter are included [4]. For this filter, the dielectric thickness was 100 nm and the critical temperature was determined to be ~ 0.5 K lower than previously reported due to more precise temperature measurement.

As can be seen from Table II, the penetration depths and critical temperatures agree to within about 3% with average values of $\lambda_0 = 303$ nm and $T_c = 12.4$ K. The differences between the penetration depth and critical temperature found for the 100-nm thick dielectric stub filter, are not surprising since the films were grown over a period of several months. Even though the growth recipe is the same, the previous history of the deposition system

TABLE I
THE LENGTH (l) AND NOMINAL WIDTHS (w) OF THE RESONANT ELEMENTS IN FIG. 1

	Interferometer		Stepped-impedance		Low-frequency stub		High-frequency stub	
	w (μm)	l (mm)						
Element 1	4	24.0	4	21.2	10	10.6	16	0.5
Element 2	4	48.0	16	21.2	8	21.2	8	1.0
Input/output line	8	3.4	8	1.4	8	1.5	8	3.3

TABLE II
PENETRATION DEPTH, CRITICAL TEMPERATURE, LOSS TANGENT, INVERSE OF THE SUPERCONDUCTING QUALITY FACTOR, AND NORMAL-STATE CONDUCTIVITY DETERMINED FROM THE TRANSMISSION CHARACTERISTICS OF THE FILTERS. $1/Q_s$ WAS COMPUTED FOR A FREQUENCY OF 1 GHz AND A TEMPERATURE OF 4.2 K

Circuit	λ_0 (nm)	T_c (K)	$\tan \delta$	$1/Q_s$	σ_n ($10^6 \Omega^{-1} \text{m}^{-1}$)
Interferometer	302	12.25	0.005	2×10^{-5}	1.7
Stepped-impedance	297	12.27	(0.005)	2×10^{-5}	(2)
Low-frequency stub	302	12.60	(0.005)	3×10^{-5}	(3)
High-frequency stub	311	12.44	(0.005)	2×10^{-5}	(2)
Previous high-frequency stub	456	13.07	0.008	1×10^{-5}	0.5

conditions the surface of the Nb target. Depending on the molecular makeup of the surface, the properties of NbCN films will be correspondingly influenced [12], [13].

While the penetration depth and critical temperature can be determined to within a few percent, the dielectric loss tangent and normal-state conductivity are more difficult to extract from the data. The difficulty arises because these quantities result from the amplitude of the transmission coefficient whereas λ_0 and T_c are determined by the location of the rejection and pass bands. The matter is further complicated by impedance mismatches at the device input and output and imperfections in the microstrip line which can set up unwanted reflections. For the results reported here, the interferometer was the only device for which values could be accurately determined. The values are $\sigma_n = 1.7 \times 10^6$ (Ωm) $^{-1}$ and $\tan \delta = 0.005$ with uncertainties of 10% and 20%, respectively. As is indicated in Table II, the loss tangent is in reasonable agreement with the value found for the high-frequency stub filter. The discrepancy in the normal-state conductivity is expected given the discrepancies that were observed for the other superconducting properties.

For the other filters, the loss parameters found for the interferometer were assumed. For the low-frequency stub filter, a σ_n of 3×10^6 (Ωm) $^{-1}$ gave a better fit to the data than the value of 2×10^6 (Ωm) $^{-1}$ found for the interferometer. This discrepancy may be a consequence of the same parasitics affecting the non-ideal behavior observed below 4 GHz. Hence, the value of σ_n extracted from the interferometer measurements is more likely to be accurate. Determining the losses for the stepped-impedance filter was complicated by the suppression in the expected transmission characteristics at ~ 3 GHz at 4.2 K. The inclusion in the model of capacitive coupling between sections of the microstrip line can partially reproduce the observed behavior. This capacitive coupling is motivated by processing problems which resulted in small islands of metalization which nearly bridge the gap be-

tween two adjacent sections of microstrip line in one of the reentrant spirals. For the high-frequency stub filter, an independent determination of the loss tangent and normal-state conductivity was not possible because of the degraded passbands. The cause of the passband degradation is not known.

B. Coplanar Transition Region

In determining the loss parameters, the type of contact to the coplanar transition region and the circuit model assumed for the transition region itself is important. For the pressure contacts, there is a capacitance and inductance associated with the exposed center pin while the impedance associated with the gold bond wires is primarily inductive. The inductance of the bond wires is on the order of 1 nH. Generally, the bond wire connections work well for frequencies below ~ 5 GHz since the capacitance is minimized. For frequencies above ~ 10 GHz, the pressure contacts are preferred since the inductance is minimized.

For the measurements of Figs. 3–6, bond wires were used for the interferometer and stepped-impedance filter and pressure contacts were used for the stub filters. For the frequency range of the interferometer and stepped-impedance filter, the inductance of the bond wires had a negligible effect on the transmission characteristics. No lumped circuit elements were included in the model to describe the transition region. The low insertion loss in Fig. 3 implies that there is little reflection due to geometric or impedance mismatch at the input and output of the circuit. The amount of ripple in the passbands indicates the degree of impedance mismatch between the microstrip lines ($\sim 28 \Omega$ at 4.2 K) and the 50- Ω cables. Considering how well the model describes the data, the observed ripple is entirely attributable to this impedance mismatch in this frequency range.

In modeling the high-frequency stub data, a series inductance was needed to describe the coplanar transition

region. The inductance was found to have two parts, a magnetic and kinetic-inductance part which had the same functional dependence as the penetration depth. The zero-temperature value of the kinetic-inductance part was ~ 0.9 nH and the magnetic part was ~ 1 nH. The use of the quartz substrates is partially responsible for this series inductance. The transition region was designed for a silicon substrate which has a larger dielectric constant. Due to processing problems with the silicon substrates, these circuits were not functional which led to the use of quartz substrates. Because of the lower dielectric constant, the coplanar section appears as a short section of high-impedance transmission line and, hence, behaves inductively.

C. Film Uniformity

While the model accurately predicts the center and side nulls of the interferometer, there is also an “in-phase” null at the center of some of the higher frequency passbands (e.g. third passband at ~ 1.2 GHz and $T = 11.1$ K). This null occurs when the phase difference between the two paths are nominally equal to integer multiples of a wavelength. Physically, this in-phase null results from a slight phase velocity difference between the signals traveling in the two arms and, hence, is most pronounced at the higher frequencies. Obvious candidates for this phase velocity difference are spatial variations in the film thicknesses, penetration depth, critical temperature, and dielectric constant, with variations in the film thicknesses thought to be the most likely.

Allowing a 3% variation in the thicknesses of the films for the two arms, the model is able to reproduce this feature, but fails to predict both the depth of the “in-phase” null or the exact frequency. At $T = 11.1$ K, the slight frequency shift is accounted for by the inadequacy of (1). While one can decrease the losses in the model to match the depth of the measured null at this frequency, the overall agreement degrades. One improvement of the model might be a gradual change in the film thicknesses between the two arms rather than the step function assumed here. An in-phase null is also observed for the higher order passbands of the low-frequency stub filter. These nulls can also be accounted for by a similar variation in the film thicknesses of the stub and trunk-line elements. From the modeled curves in Fig. 5, one can see that these nulls (e.g. ~ 8.0 and 8.8 GHz at $T = 4.31$ K) are reasonably well described.

Spatial variation in the film thicknesses can also explain the asymmetry seen in the secondary passbands located between a side and center null of the interferometer. The thickness variation results in an impedance variation between the two arms and, hence, affects the shape of the passband. As was the case for the “in-phase” null, one finds that the amount of loss improves the agreement for the secondary bands while degrading the overall fit.

Considering that the circuit size is small fraction of the 15 cm-diameter sputtering targets used for growing the films, a 3% variation in the film thickness may not seem reasonable. However, a spatial variation in the “pin-hole”

density of the dielectric may cause an “effective” variation in the film thicknesses. As was pointed out in Section II, the dielectric layers were deposited in two steps. Following this procedure, the pin-hole shorts formed in the first half of the dielectric are unlikely to overlap with those formed in the second half of the dielectric. While shorts between the superconducting layers have been avoided, the thickness of the film will be $\sim d_d/2$ over a small percentage of the circuit area creating an “effective” dielectric thickness. Since one has little control over how these pin-hole shorts are distributed, the spatial variation found in the model appears to be reasonable.

The spatial thickness variation also accounts for the small discrepancies mentioned above for the penetration depth. Since the phase velocity contains the ratio λ_0/d_s and λ_0/d_t , any uncertainty in the film thicknesses translates into an uncertainty for the penetration depth λ_0 . The 3–6% thickness variation proposed for the interferometer and low-frequency stub certainly allows for the 3% uncertainty in the penetration depth. For the 3% critical temperature discrepancy, similar arguments also apply.

IV. CONCLUSION

The agreement obtained between the modeled and measured data show that the parallel-plate characterization of the superconducting microstrip lines can accurately predict the microwave properties of the circuits. The agreement between the penetration depths, critical temperatures, and loss parameters also supports this claim. The device characteristics are nevertheless quite susceptible to circuit imperfections indicating the need for better control of the fabrication process which would also increase the yield of the devices.

An important result of this investigation is to quantify the degree of film uniformity achievable with our present deposition technology and photolithographic processing. The presence of an “in-phase” null in the transmission characteristics of the interferometer and low-frequency stub indicate that there was a 3–6% spatial variation in the “effective” film parameters which affects the phase velocity. This spatial variation is thought to be the result of pin holes in the dielectric layer. The density of pin holes might be reduced by using a dielectric layer that is better lattice matched to NbCN such as MgO. The use of a clean-room facility would also significantly reduce the amount of dust available for pin-hole sites. Obviously, to design and fabricate narrow-band filters, significant improvements in the film-thickness variation are required.

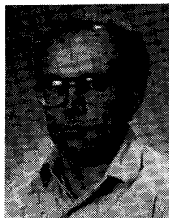
The dissipation losses of the devices tested were limited by the hydrogenated-silicon dielectric for temperatures well below the critical temperature. As indicated in Fig. 2, a loss tangent of 0.0001 is necessary to be limited by the superconducting losses at a reduced temperature of 0.3 and 10 GHz. This value represents a 50 times reduction over that found for a-Si:H which might be achieved with magnesium oxide (MgO) as the dielectric. The benefits of using MgO are that it grows epitaxially on niobium nitride

[14] and, in its bulk form, the loss tangent is in the desired range [10].

The insertion loss due to impedance and geometric mismatch for these microstrip structures has also been discussed. Using (4), the characteristic impedance of the input lines was $\sim 30 \Omega$ at 4.2 K. The $30\text{-}\Omega$ impedance of the interferometer is responsible for the relatively low reflected power. To achieve a better match it will be necessary to fabricate $50\text{-}\Omega$ kinetic-inductance microstrip lines which will require accurate control of the penetration depth and line width. For the geometric mismatch, the interferometer data showed that the coplanar transition region successfully minimized these effects for frequencies below 2 GHz. For higher frequency devices, further refinement of the transition-region design will be necessary to eliminate the parasitic series inductance required in the model of the high-frequency stub filter. The high-frequency design is a nontrivial problem that is presently hampered by the unavailability of three-dimensional electromagnetic field solving programs that properly model thin-film superconductors.

REFERENCES

- [1] J. M. Pond, J. H. Claassen, and W. L. Carter, "Kinetic inductance microstrip delay lines," *IEEE Trans. Magn.*, vol. 23, pp. 903-907, Mar 1987.
- [2] —, "Measurements and modelling of kinetic inductance microstrip delay lines," *IEEE Trans. Microwave Theory Tech.*, vol. 35, pp. 1256-1262, Dec. 1987.
- [3] P. V. Mason and R. W. Gould, "Slow-wave structures utilizing superconducting thin-film transmission lines," *J. Appl. Phys.*, vol. 40, pp. 2039-2051, Apr. 1969.
- [4] J. M. Pond, K. R. Carroll, and E. J. Cukauskas, "Ultra-compact microwave filters using kinetic inductance microstrip," *IEEE Trans. Magn.*, vol. 27, pp. 2696-2699, Mar. 1991.
- [5] T. Van Duzer and C. W. Turner, *Principles of Superconductive Circuits*, New York: Elsevier, 1981.
- [6] J. C. Swihart, "Field solution for a thin-film superconducting strip transmission line," *J. Appl. Phys.*, vol. 32, pp. 461-469, Mar. 1961.
- [7] J. M. Pond, K. R. Carroll, J. S. Horwitz, D. B. Chrisey, M. S. Osofsky, and V. C. Cestone, "Penetration depth and microwave loss measurements with a $\text{YBa}_2\text{Cu}_3\text{O}_{7.8}/\text{LaAlO}_3/\text{YBa}_2\text{Cu}_3\text{O}_{7.8}$ trilayer transmission line," *Appl. Phys. Lett.*, vol. 59, pp. 3033-3035, Dec. 1991.
- [8] J. M. Pond, P. F. Weaver, and I. Kaufman, "Propagation and circuit characteristics of inductively coupled superconducting microstrip," *IEEE Trans. Microwave Theory Tech.*, vol. MTT-38, no. 11, pp. 1635-1643, Nov. 1990.
- [9] D. P. McGinnis and J. B. Beyer, "A broad-band microwave superconducting thin-film transformer," *IEEE Trans. Microwave Theory Tech.*, vol. 36, pp. 1521-1525, Nov. 1988.
- [10] T. Konaka, M. Sato, H. Asano, and S. Kubo, "Relative permittivity and dielectric loss tangent of substrate materials for high- T_c superconducting film," *J. Superconductivity*, vol. 4, pp. 283-288, 1991.
- [11] E. J. Cukauskas, W. L. Carter, and S. B. Qadri, "Superconducting and structure properties of niobium nitride prepared by rf magnetron sputtering," *J. Appl. Phys.*, vol. 57, pp. 2538-2542, Apr. 1985.
- [12] E. J. Cukauskas, "The effects of methane in the deposition of superconducting niobium nitride thin films at ambient substrate temperature," *J. Appl. Phys.*, vol. 54, pp. 1013-1017, Feb. 1983.
- [13] S. A. Wolf, I. L. Singer, E. J. Cukauskas, T. L. Francavilla, and E. F. Skelton, "Effects of deposition parameters on the properties of superconducting rf reactively sputtered NbN films," *J. Vac. Sci. Technol.*, vol. 17, pp. 411-414, Jan. 1980.
- [14] J. Talvacchio and A. I. Braginski, "Tunnel junctions fabricated from coherent NbN/MgO/NbN and NbN/ Al_2O_3 /NbN structures," *IEEE Trans. Magn.*, vol. 23, pp. 859-862, Mar. 1987.



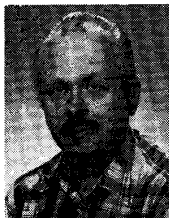
Kenneth R. Carroll received the Ph.D. degree from the University of Maryland in Physics in 1987.

From 1987 to 1990 he was a Faculty Research Associate in the Experimental General Relativity Group at Maryland. The research concerned the implementation of dc SQUIDS and superconducting transducers to cryogenic gravity wave detectors. Since 1990 he has been at the Naval Research Laboratory, Washington, DC in the Microwave Technology Branch as a National Research Council Research Associate. At the laboratory, his investigations have concerned the application of superconducting and active-dielectric thin films in multilayer structures for microwave devices.



Jeffery M. Pond was born in South Haven, MI in 1956. He received the B.S. degree in electrical engineering from Michigan State University in 1978 and the M.S. and Ph.D. degrees in electrical engineering from the University of Michigan in 1979 and 1982, respectively.

From 1979 to 1982 he was a Research Assistant in the Radiation Laboratory at the University of Michigan, where his research involved electromagnetic scattering and inverse scattering. In 1982, he joined the Microwave Technology Branch of the Naval Research Laboratory, Washington, DC. His research interest there have focused mainly on the investigation of novel device and circuit concepts using thin-film superconductors.



Edward J. Cukauskas was born in Philadelphia, PA, in 1942. He received the B.S. and M.S. degrees in Physics from the University of Scranton, PA, in 1968 and 1970, respectively, and the Ph.D. degree in physics from the University of Virginia in 1974.

From 1974 to 1977, he was a Radiation Effects Analyst at the BDM Corp., McLean, VA. In 1977, he joined the Applied Superconductivity Section at the Naval Research Laboratory, Washington, DC. There his research interests focused on refractory superconducting materials and tunneling device studies. Presently, his research interests are concentrated on the copper oxide high temperature superconducting materials and Josephson effect devices.